

length of 6.2 m, and QD0 (shown in figure 3), which has an aperture radius of just 4.125 mm. Moreover, the field in the QD0 aperture is the most relevant quantity, but due to meshing convergence problems, and to computation time, the precision of the results is lower than the one achievable by models representing the single magnet only.

Finally, due to the *hybrid* design of QD0 [2], permanent magnets, soft ferromagnetic region, normal conducting racetrack coils and super-conducting solenoids have to be included all at once in the same simulation.

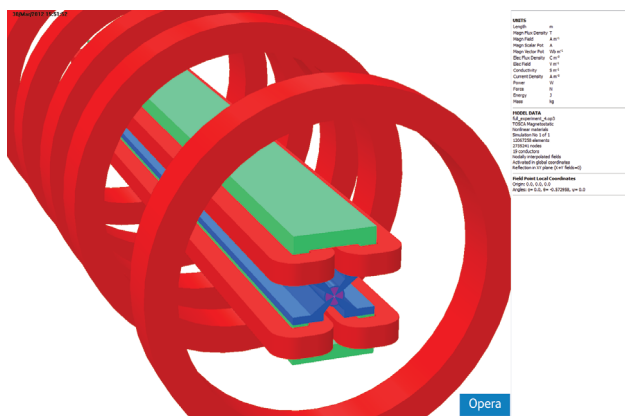


Figure 3: A detail of QD0 inside the anti-solenoid.

Results

In terms of field on the beam axis, the resulting component B_z is plotted in figure 4, and B_r is shown in figure 5. The effect of QD0 on the beam axis is beneficial, since its ferromagnetic structure *shields* the beam from the surrounding fields. Such results are visibly affected by a numeric error due to the element size, so they were averaged before being used for beam dynamics simulations. This averaging may appear unjustified, but it was necessary, considering the nature of the problem and the FE model features. The luminosity loss due to the new field maps is

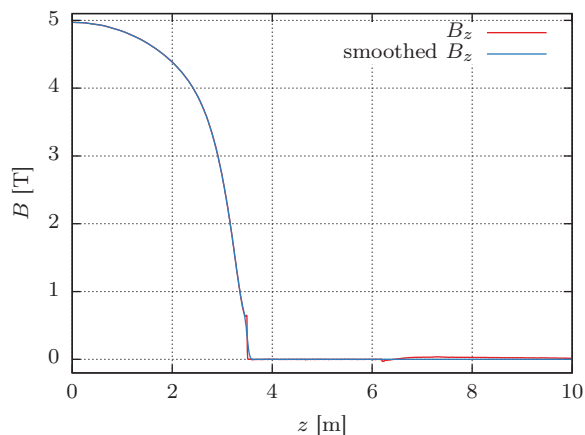


Figure 4: Axial component of the field on the beam axis.

$\simeq 14\%$, which is compatible with any other previous CLIC SiD design simulated so far [3].

Finally, such model permitted to evaluate the forces acting on the anti-solenoid, which are not affected by the introduction of QD0, and remained equal to the ones evaluated in the 2D case: the most relevant is the axial force F_z of $7.0 \cdot 10^6$ N acting on the first coil of the anti-solenoid, pushing it away from the IP.

THE QD0 IN DETAIL

As already anticipated, one of the most noticeable advantage of the whole 3D simulation is the possibility to study in detail the interactions between QD0 and the detector magnetic field. This permitted to improve the anti-solenoid design established with 2D simulations, by adjusting its current in order to balance the higher field attracted by the QD0 in the yoke end-cap region.

This adjustment consisted in an iterative process in which new coil dimensions and currents of the anti-solenoid were proposed, simulated and then evaluated by comparing the performance of QD0 in the different cases. During such procedure it was noticed that without making any change in the overall layout, the innermost area of QD0 could be unable to develop the required gradient. Figure 6 shows the axial field attracted by the QD0 in case of an anti-solenoid layout compatible with the CLIC baseline. Such results (up to 3 T of external field entering the QD0 poles) are not compatible with the correct functioning of the magnet, so a solution is being proposed.

A Proposed Solution

A better QD0 performance was achieved by moving the anti-solenoid towards the IP and adjusting its coil shapes and currents [1]. Figure 7 shows the field attracted by QD0 in this solution, while the gradient it developed across its length is plotted in figure 8. Such gradient is measured along four lines parallel to the beam axis, placed at a distance of 1 mm from it either in the $\pm x$ or the $\pm y$ directions. A slight decrease of the gradient in the innermost region of

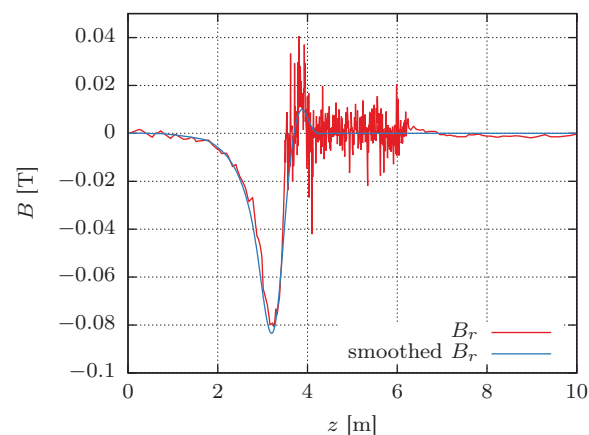


Figure 5: Radial component of the field on the beam axis.

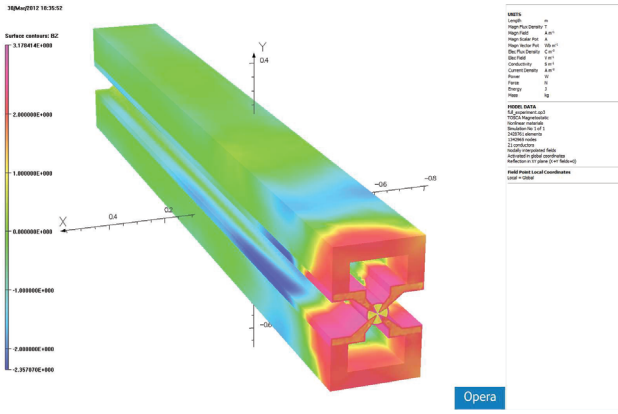


Figure 6: The axial field in the QD0 structure.

the magnet is still visible, but the integrated gradient differed by less than 5% from the requirements, which is acceptable given the R&D status of the detector study.

This case was also studied by the mechanical point of view, and the magnetic forces acting on QD0 are estimated as $F_z \simeq -5.7$ kN, $F_x \simeq 8.3$ kN and $T_y \simeq 5.6 \cdot 10^3$ Nm.

Finally, to demonstrate the efficiency of the anti-solenoid solution, a last configuration was investigated, not intended to be compliant with the CLIC beam delivery system baseline, as it is based on an L^* increased by 0.3 m (from 3.5 m to 3.8 m). The QD0 gradient obtained is plotted in figure 9, and its integral differs by less than 1% to the specifications, which is less than the accuracy of the model itself.

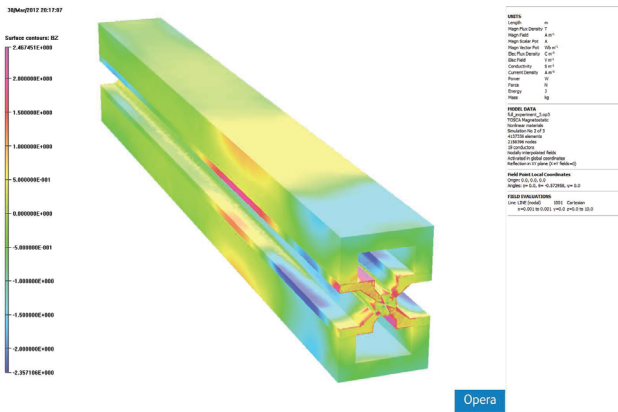


Figure 7: The axial field in the QD0 structure, with the newly proposed anti-solenoid.

CONCLUSIONS

The most important achievement of this study was that with an appropriate shielding (i.e. the anti-solenoid) the QD0 can work as specifications, even if placed very close to the strong detector magnetic field. On the other hand, to obtain such performances it is necessary an adequate space allocation. A proper shielding of the QD0 also reduces the forces acting on this hybrid electromagnet, making its stabilization easier. Finally, regarding the impact of such sys-

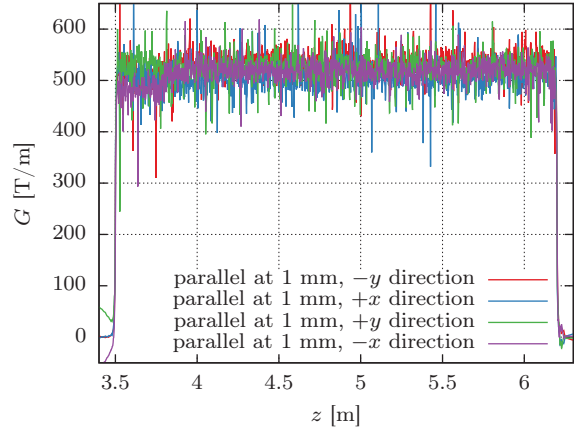


Figure 8: QD0 gradient on four parallels to the beam axis.

tems on the incoming beam, it can be noticed that the luminosity loss is *coherent* with all the previous designs and it is related mainly to the radial component of the field in the region between QD0 and the IP.

ACKNOWLEDGMENT

A sincere thanks goes to the whole MDI working group, especially to L. Gatignon the detector team, represented by A. Gaddi and H. Gerwig and also to the beam dynamic team, represented by B. Dalena.

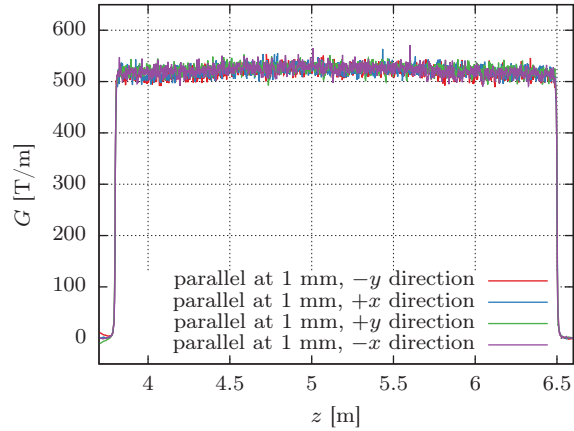


Figure 9: QD0 gradient on axis parallels, with $L^* = 3.8$ m.

REFERENCES

- [1] A. Bartalesi and M. Modena, "Design of an Anti-Solenoid System for the CLIC SiD Experiment" CERN TE-MSC Internal Note 2012-11, EDMS Nr. 1214775.
- [2] M. Modena et al., "Design, Assembly and First Measurements of a Short Model for CLIC Final Focus Hybrid Quadrupole QD0", this conference.
- [3] B. Dalena, "CLIC main detector solenoid and anti-solenoid impact" Presented at the CERN CLIC Collaboration Working Meeting, 10 May 2012.